RSC Advances

ROYAL SOCIETY OF CHEMISTRY

www.rsc.org/advances

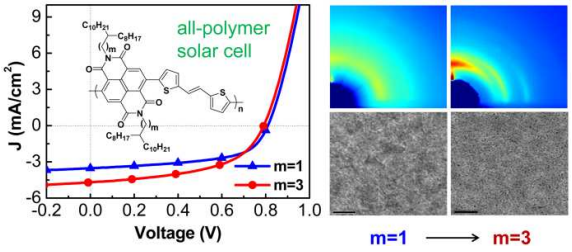

The improved performance was attributed to the well-ordered structure of polymer C3 and nanoscale phase separation in blend film, which was originated from the manipulating the alkyl-chain branching position of polymer.

Journal Name

RSCPublishing

ARTICLE

Effect of Alkyl-Chain Branching Position on Nanoscale Morphology and Performance of All-Polymer Solar Cells

Cite this: DOI: 10.1039/x0xx00000x

Received 00th January 2012,
Accepted 00th January 2012

DOI: 10.1039/x0xx00000x

www.rsc.org/

Fangbin Liu,[ab] Hui Li,[ab] Chunling Gu*[b] and Hongbing Fu*[b]

Manipulating the alkyl-chain branching position afforded two naphthalenediimide-based polymers (C1 and C3). The optoelectronic properties including the absorption spectra and electronic energy levels, conformations and photovoltaic properties of two polymers were fully studied and compared. The effect of alkyl-chain branching position on their optoelectronic properties and crystallinity were investigated in detail. Moving the branching position away from the backbone resulted in superior crystallinity of C3. All-polymer solar cells (all-PSCs) based on C1 or C3 as the acceptor and polymer PBDTTT-C-T as the donor were fabricated and optimized. The power conversion efficiencies (PCEs) of the optimized all-PSCs based on C1 and C3 reached 1.68% and 1.92%, respectively. The improved photovoltaic performance may be due to the clear nanoscale morphology of C3-based blend film. The blend film exhibits favorable phase separation and well ordered structure of polymer C3. This largely increased the electron mobility (up to 1.0×10^{-4} cm^2 V^{-1} s^{-1}) which contributes to balancing the charge transport in C3-based blend film. This is the first report on realization of favorable phase separation and high electron mobility through improvement of acceptor crystallinity in all-PSCs.

Introduction

All-polymers solar cells (all-PSCs) have received much attention in recent years, as they provide a facile and low-cost way to utilize solar energy.[1-4] π-conjugated polymers as acceptor materials in all-PSCs have potential advantages. In comparison with fullerene derivatives, π-conjugated polymers can be easily chemically synthesized and modified. They have broad absorption spectrum and high absorption coefficiency, and possess fine-tuned energy levels to match the donor polymer.[4-7] However, all-PSCs are still being advanced slowly with low power conversation efficiency (PCE), for example, the performance based on the backbones of naphthalene diimide (5.7%)[8], perylene diimide (4.4%)[9], fluorene (2.0%)[7,10], and carbazol(3.68%)[11]. The relatively low efficiency has been considered to be due to the unfavorable morphology of BHJ blend films such as small phase[12] and reduced ordering of polymer chains[13]. A significant challenge for π-conjugated polymers as acceptor alternatives to replace fullerene derivatives is to improve the phase separation and charge transport ability[14]. Therefore, the acceptor polymer with high crystallinity or aggregation ability is highly desired, similar to fullerene derivatives[14-16], to realize high phase separation and electron mobility in all-PSCs.

From the point of molecular design, polymer crystallinity is significantly related to the planarization of polymer backbones which could be achieved by modulating the molecular structure of π-functional backbone and the pattern of alkyl side chains.[17,23] The latter has been widely accepted to impact on the morphology (crystallization, π-stacking and packing orientation), charge transport and photovoltaic performance of devices.[24-27] Kazuo Takimiya group studied that different linear and branched alkyl side chains altered the polymer orientation, thus affecting the PCEs of device.[28] It should be mentioned that previous investigations are limited to the study of donor polymers' alkyl chains including alkyl chain length and branching point[29-35]; however, the effect of alky-chain brancing position in acceptor polymers on the performance has not been reported in all-PSCs. Detail studies on the critical role of alkyl chain on photovoltaic performance of all-PSCs are thus highly desired. Furthermore, the manipulation of alkyl-chain branching position should be an important strategy to design polymers with good crystallinity and achieve high performance as acceptor in all-PSCs.

Due to highly electron-deficient character of Naphthalene diimide (NDI)[36-37], NDI-based derivatives possess deep low unoccupied molecular orbital (LUMO) energy levels, which make them good electron transporting semiconductors and

suitable acceptor materials for PSCs. As a result, NDI-based copolymers have attracted much attention in the fields of PSCs and organic field effect transitors (OFETs).[4,37-43] Among these works, a typical NDI-bithiophene copolymer (PNDI-TT) with good aggregation ability was initially proved to exhibited low efficiencies of 0.2−1.4% PCE in all-PSCs.[42-46] Very recently, Shinzaburo Ito group reported high PCE above 4% based on the same polymer as acceptor via significantly enhancing charge-carrier generation and collection efficiencies.[8,47] At the same time, Liu et al reported that the introduction of vinyl group into the copolymer backbone of PNDI-TT could improve the charge mobility of neat film in OFET during our work.[38] It is proved that vinyl group can extend the polymer coplanarity as well as the intermolecular π-π stacking, which would enhance the polymer crystallinity with negligible influence on the low-lying LUMO energy level. Herein we focus on the manipulation of branching position of the alkyl chain to improve crystallinity, which would be beneficial to increase the PCE via favorable phase separation in all-PSCs.

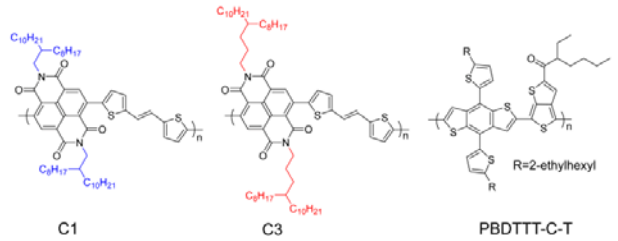

Fig. 1 Chemical structures of polymers C1, C3 and donor polymer PBDTTT-C-T.

In this study, we had successfully designed and synthesized C1 and C3, where Cm referred to the number of linear carbon atoms between the alkyl-chain branching position and the alkylated nitrogen (Fig. 1). A systematic study of their optical, electronic, conformation properties, and the characteristics of all-PSCs based on these polymers were described. By contrast research, a detailed structural analysis of these polymers was performed using grazing incidence X-ray diffraction (GIXD) and transmission electron microscopy (TEM) to elucidate the effect of the branching position on polymer crystallinity and morphology of the blend film. It was found that the morphologies of all-polymer BHJ films strongly depend on the alkyl-chain branching position. Better device performance was obtained from polymer C3 with superior crystallinity where a PCE of 1.92% was obtained under AM 1.5G illumination with 3% 1,8-diiodooctane (DIO) as processing additive. The improved performance arises from the clear nanoscale morphology with favorable phase separation and well ordered domians. Our results provide an example for rational design criteria of polymer acceptor to realize nanoscale phase separation morphology and high electron mobility.

Experimental section

Materials

The polymers PBDTTT-C-T were purchased from Solarmer Materials Inc. and used as received. The number-average-molecular-weight (M_n), and polydispersity index (PDI; given by M_w/M_n, where M_w is the weight-average-molecular-weight) provided on the Certificate of Analysis were 54.9 kg mol^{-1} and 1.9, respectively. 2-(tributylstannyl)thiophene, NBS, trans-1,2-bis(tributylstannyl)ethene were purchased from Sigma-Aldrich. Compounds 2-octyldodecan-1-amine (2a) and 4-octyltetradecan-1-amine (2b) were purchased from LYN (Beijing) technology Co. Ltd.. Compound 2,6-dibromo-1,4,5,8-Naphthalene tetracarboxylic dianhydride (1) was synthesized according to the literature.[36-37] Toluene was dried over Na/benzophenoneketyl and freshly distilled before use. The other reagents and solvents used in this work were commercially purchased and used without further purification. All air and water sensitive reactions were performed under nitrogen atmosphere. The detailed synthetic processes of the other compounds are as follows.

Synthetic procedures

N,N'-bis(4-octyltetradecyl)-2,6-dibromo-1,4,5,8-naphthalene Diimide (3b). A mixture of 1 (2.12 g, 5.0 mmol), 4-octyltetradecyl amine (4.07 g, 12.5 mmol), and acetic acid (100 mL) was stirred at 110 °C for 12 h. After cooling to room temperature, most of solvent was removed in vacuum, and the residue was purified by column chromatography on silica gel with a mixture of ethyl acetate/petroleum ether (1:60, v/v) as eluent, affording a slightly yellow solid as the product (1.30 g, 1.25 mmol, yield 25%). ^{1}H NMR ($CDCl_3$, 400 MHz) δ: 8.98 (s, 2H), 4.16 (d, J = 7.6 Hz, 4H), 1.70 (m, 4H), 1.32-1.41 (m, 6H), 1.15-1.35 (m, 64H), 0.85-0.89 (m, 12H) ; ^{13}C NMR ($CDCl_3$, 400 MHz) δ: 160.60, 138.97, 128.27, 127.60, 125.28, 124.01, 77.45, 77.03, 76.61, 41.49, 37.22, 33.54, 31.93, 30.96, 30.10, 29.71, 29.66, 29.37, 26.67, 25.15, 22.69, 14.13; MS-TOF[M]$^+$: 1040.5 (m/z).

N,N'-bis(2-octyldodecyl)-2,6-dibromo-1,4,5,8-naphthalene Diimide (3a). A mixture of 1 (1.92 g, 4.5 mmol), 2-octyldodecan-1-amine (3.35 g, 11.25 mmol), and acetic acid (90 mL) was stirred at 110 °C for 12 h. Slightly yellow solid (1.37 g, 1.40 mmol, yield 31%) was obtained with the same processing method as compound 3a. ^{1}H NMR ($CDCl_3$, 400 MHz) δ: 8.95 (s, 2H), 4.12 (d, J = 7.5 Hz, 4H), 1.97 (m, 2H), 1.20-1.40 (m, 64H), 0.84-0.89 (m, 12H); MS-TOF[M]$^+$: 984.5 (m/z).

N,N'-Bis(4-octyltetradecyl)-2,6-bis([2,2']-bithiohenyl-5-yl)-1,4, 5,8-naphthalene Diimide (4b). 3b (1.04 g, 1.0 mmol), 5-tributylstannyl-2,2'-bithiophene (0.94 g, 2.5 mmol), $Pd(PPh_3)_2Cl_2$ (98 mg, 0.1 mmol) and 20 mL of anhydrous toluene were added to a flask under argon. The mixture was refluxed for 16 h and then cooled down to room temperature. After quenching with $CaF_2{\cdot}12H_2O$, the solvent was removed under vacuum and the product was purified by column flash chromatography using an ethyl acetate/petroleum ether solvent mixture (10:1). The pure product was obtained as a red solid (943 mg, 0.9 mmol, yield 90%). ^{1}H NMR ($CDCl_3$, 400 MHz) δ: 8.77 (s, 2H), 7.78 (d, 4H), 7.31 (d, 2H), 7.21 (d, 2H), 4.10(d, J

= 7.6 Hz, 4H), 1.70 (m, 4H), 1.32-1.41 (m, 6H), 1.15-1.35 (m, 64H), 0.85-0.89 (m, 12H). ^{13}C NMR ($CDCl_3$, 400 MHz) δ: 162.13, 161.96, 140.73, 140.28, 136.62, 128.85, 127.94, 127.46, 127.39, 125.43, 123.47, 77.34, 77.03, 76.71, 41.48, 37.31, 33.58, 31.92, 31.01, 30.11, 29.69, 29.65, 29.35, 26.68, 25.34, 22.68, 14.10; MS-TOF[M]$^+$: 1046.8 (m/z).

N,N'-Bis(2-octyldodecyl)-2,6-bis([2,2']-bithiohenyl-5-yl)-1,4,5,8-naphthalene Diimide (4a). 3a (1.37 g, 1.4 mmol), 5-tributylstannyl-2,2'-bithiophene (1.32 g, 3.5 mmol), $Pd(PPh_3)_2Cl_2$ (137.2 mg, 0.14 mmol) and 20 mL of anhydrous toluene were added to a flask under argon. Red solid (1.24 g, 1.25 mmol, yield 89%) was obtained with the same processing method as compound 4a. ^{1}H NMR ($CDCl_3$, 400 MHz) δ: 8.74 (s, 2H), 7.54 (d, J = 5.1 Hz, 2H), 7.28 (d, J =3.6 Hz, 2H), 7.18 (m, 2H), 4.05 (d, J = 7.2 Hz, 4H), 1.93 (m, 2H), 1.23 (m, 64H), 0.86 (m, 12H); MS-TOF[M]$^+$: 990.8 (m/z).

N,N'-Bis(4-octyltetradecyl)-2,6-bis(5-bromo-thiophenyl-5-yl)-1,4,5,8-naphthalene Diimide (5b). 4b (524 mg, 0.5 mmol) was dissolved in 25 mL of chloroform. NBS (214 mg, 1.2 mmol) was added to the reaction mixtures. After stirring in the dark for two days, the product was extracted with dichloromethane and washed with brine, and the organic layer was evaporated. The red solid was purified by column chromatography using an ethyl acetate/petroleum ether (1:50) solvent mixture to give the final product as red solid (493 mg, 0.41 mmol , yield 82%). ^{1}H NMR ($CDCl_3$, 400 MHz) δ: 8.72 (s, 2H), 7.15 (d, J = 3.9 Hz, 2H), 7.08 (d, J= 3.9 Hz, 2H), 4.10 (d, J = 5.6 Hz, 4H), 1.55 (m, 4H), 1.24 (m, 64H), 0.85-0.87 (m, 12H); ^{13}C NMR ($CDCl_3$, 400 MHz) δ: 161.89, 142.05, 139.11, 136.44, 130.18, 128.85, 127.50, 125.63, 123.21, 115.50, 77.47, 77.05, 76.62, 41.57, 37.27, 33.55, 31.94, 30.99, 30.12, 29.71, 29.67, 29.37, 26.67, 25.32, 22.70,14.14; MS-TOF[M]$^+$: 1205.4 (m/z).

N,N'-Bis(2-octyldodecyl)-2,6-bis(5-bromo-thiophenyl-5-yl)-1,4,5,8-naphthalene Diimide (5a). 4a (1.09 g, 1.1 mmol) was dissolved in 25 mL of chloroform. NBS (235.0 mg, 1.32 mmol) was added to the reaction mixtures. Red solid (1.08 g, 0.935 mmol, yield 85%) was obtained with the same processing method as compound 5a. ^{1}H NMR ($CDCl_3$, 400 MHz) δ: 8.77 (s, 2H), 7.44 (d, J = 3.9 Hz, 2H), 7.08 (d, J= 3.9 Hz, 2H), 4.07 (d, J = 7.2 Hz, 4H), 1.94 (m, 2H), 1.24 (m, 64H), 0.85 (m, 12H); MS-TOF[M]$^+$: 1148.4 (m/z).

Preperation of Poly[N,N'-bis(4-octyltetradecyl)-2,6-bis-([2,2']-bithiophenyl-5-yl)-1,4,5,8-naphthalenediimide-5',5 -diyl]-alt-trans-ethylene (C3). 5b (120.5 mg, 0.1 mmol), trans-1,2-bis(tributylstannyl)ethane (6.6 mg, 0.1mol), $Pd_2(dba)_3$ (9.2 mg, 0.01mol), P(*o*-tol)$_3$ (12.2 mg, 0.04mol) and 3 mL of toluene were added to a Schlenk tube. The tube was charged with nitrogen through a freeze-pump-thaw cycle for three times. The mixture was stirred for 48 h at 110 °C. The mixture was cooled to room temperature and precipitated into methanol (100 mL). The precipitate was filtered through a nylon filter, purified via Soxhlet extraction for 12 h with methanol, acetone, hexane, chloroform, and chlorobenzene, and finally collected with dichlorobenzene. The dichlorobenzene solution was then concentrated by evaporation, precipitated into methanol (100 mL), and filtered off to afford a dark blue solid (77.5 mg, yield 61%).

Poly [N,N'-bis(2-octyldodecyl)-2,6-bis(thiophenyl-5-yl)-1,4,5,8-naphthalene diimide-2,2'-diyl]-alt-trans-ethylene (C1). 5a (229.8 mg, 0.20 mmol), trans-1,2-bis(tributylstannyl)ethane (13.2 mg, 0.20mol), $Pd_2(dba)_3$ (18.2 mg, 0.02mol), P(*o*-tol)$_3$ (24.2 mg, 0.08mol) and 5 mL of toluene were added to a Schlenk tube. The same processing method as polymer C3 was done in during the polymerization and purification. After the Soxhlet extraction, product was finally collected with chlorobenzene. Dark blue solid, 147.4 mg, yield 58%.

Measurements and Characterization

^{1}H NMR spectra and ^{13}C NMR spectra were measured on a Bruker DMX-400 spectrometer in $CDCl_3$ (^{1}H, δ: 7.26 ppm; ^{13}C, δ: 77 ppm) with trimethylsilane (TMS) as the internal standard. Gel permeation chromatography (GPC) was performed on Polymer Laboratories PL 220 at 150 °C using 1,2,4-tricholorobenzene (TCB) as eluent. The obtained molecular weight is calibrated with the polystyrene standard. Thermal gravity analyses (TGA) were investigated using a TA Instrument NETZSCH STA 409 PC/PG analyzer operated at a heating rate of 10 ^{o}C min^{-1} and under a nitrogen atmosphere. UV-visible (UV-vis) absorption spectra were taken on a Shimidazu UV-3600 UV-vis-NIR spectrophotometer. The structural property of polymer was determined by GIXD measurements on the thin film produced by dropping polymers' DCB solution onto Si substrate. The thickness of the functional layers was measured using a KLA-T encore P-6 profilometer (Tencor). The morphology and surface roughness of the layers were determined by atomic-force microscopy (AFM, Digital Instruments Nano Scope III). Transmission electron microscopy (TEM) images were taken on a JEM-2100 transmission electron microscope operated at an acceleration voltage of 200 kV. The sample used in AFM and TEM measurement is from the naked active layer in devices. Cyclic voltammetry measurements were performed on a Zahner IM6e electrochemical workstation with a three-electrode system in a solution of 0.1 M Bu_4NPF_6 in anhydrous acetonitrile at a scan rate of 50 mV s^{-1}.

PSC Device Fabrication and Measurement

The PSC devices were fabricated with a structure of ITO/PEDOT:PSS/active layer/Ca/Al, where the active layer is composed of C1 or C3 as acceptor and polymer PBDTTT-C-T as donor. Patterned ITO-glass substrates were used as the anode in polymer solar cells. ITO substrates were firstly pre-cleaned sequentially by sonicating in a detergent bath, de-ionized water, acetone, and isopropanol each for 20 min, and then dried in an oven for 30 min, which were then subjected to a UV/ozone treatment for 60 min. A thin layer of PEDOT:PSS (poly(3,4ethylenedioxythiophene):poly (styrenesulfonate)) was spin-casted onto the ITO surface. After being baked at 150 °C for 20 min in ambient air, the substrates were transferred into a nitrogen-filled glove box (<0.1 ppm O_2 and H_2O). C1 or C3

was blended with polymer PBDTTT-C-T and dissolved in 1,2-dichlorobenzene (*o*-DCB). The active layers were then spin-cast from the blend solutions (20 mg/mL, polymer weight concentration) with various rotational speeds on the ITO/PEDOT:PSS substrates. A small amount of DIO was used as an additive to improve the photovoltaic performance of the devices if necessary. Beside this, no further treatment to the blend film was performed before the deposition of the metal electrode. Finally, a Ca/Al metal top electrode was deposited under vacuum onto the active layer at a pressure of ca. 5×10^{-5} Pa. The active area of the device was ca. 6.0 mm^2. The current density-voltage (*J-V*) characteristics were measured on a computer-controlled Keithley 2400 Source Measure Unit. A xenon lamp coupled with an AM 1.5 solar spectrum filter was used as the light source, and the optical power was 100 mW cm^{-2}. The EQE measurements of the encapsulated devices were performed in air (PV Measurements Inc., Model QEX7). The hole and electron mobilities was calculated by fitting the dark J-V curves for the hole-only and electron-only devices to the space-charge-limited-current (SCLC) model at low voltages.

Results and discussion

Synthesis and Characterization

The synthetic routes of the monomers and corresponding polymers are outlined in Scheme 1. Polymers C1 and C3 were synthesized by Stille coupling reaction between the dibromide monomers (3a and 3b) and the trans-1,2-bis (tributylstannyl)ethene using $Pd_2(dba)_3$ as the catalyst. The obtained polymers were precipitated in methanol and then purified by Soxhlet extraction to remove oligomers and other impurities. The number average molecular weights (M_n) and polydispersity indices (PDIs) were 23.0 kDa and 3.5, 74.5 kDa and 2.7, for C1 and C3 respectively, evaluated by high temperature gel permeation chromatography at 150 °C using the

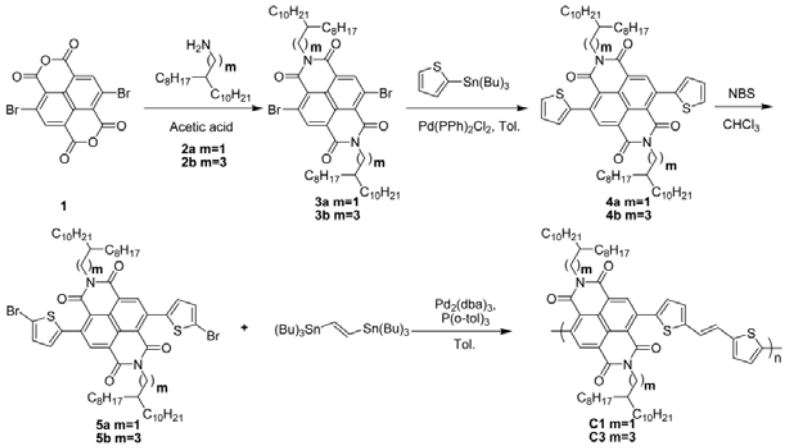

Scheme 1 Synthesis routes of the monomers and conjugated polymers C1 and C3

Table 1 Basic Properties of Polymers (Molecular Weights, Thermostability, Optical and Electrochemical Properties).

Cn	M_n[a] (kDa)	M_w[a] (kDa)	PDI[a]	T_d[b] (°C)	λ_{max}[c] (nm)	λ_{max}[d] (nm)	λ_{onset}[d] (nm)	E_g^{opt}[e] (eV)	E_{HOMO} (eV)	E_{LUMO} (eV)
C1	23.0	79.9	3.5	433	395, 678	403, 716	890	1.40	-5.61	-3.93
C3	74.5	197.8	2.7	445	396, 684	405, 726, 805	895	1.38	-5.61	-3.94

[a]Determined by GPC in trichlorobenzene at 150 °C using polystyrene standards. [b]Decomposition temperature, determined by TGA in nitrogen at a heating rate of 10 °C/min, based on 5% weight loss. [c]Measured in dilute toluene solution. [d]Spin-casted from 4 mg/mL dichlorobenzene solution. [e]Optical band gap calculated from the onset of film absorption.

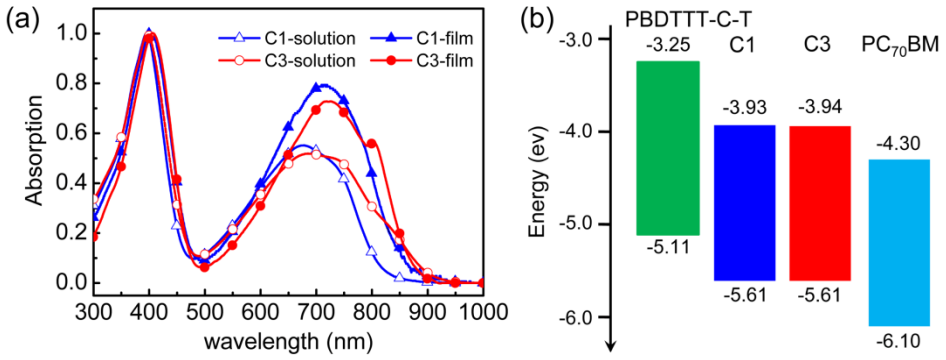

Fig. 2 (a) Normalized UV-vis absorption spectra of C1 and C3 in toluene solution and thin films. (b) HOMO and LUMO energy levels of the polymers and $PC_{70}BM$.

1,2,4-tricholorobenzene as the eluent. The two polymers had molecular weights more than 20 kg/mol, which is considered to be quite high for low bandgap polymers.[48-50] In our work, the effect of molecular weight of two polymers is a negligible factor according to the similar performance of BHJ solar cells in unoptimized devices. The thermogravimetric analysis measurements (TGA) showed that the onset temperatures (T_d) of C1 and C3 with 5% weight-loss are all over 430 °C.

Optoelectronic and Electrochemical Properties

The optical properties of C1 and C3 were measured in toluene solution and thin film (Fig. 1), and the detailed absorption data were collected and listed in Table 1. Those polymers show similar broad absorption spectral features across the entire UV-vis region in toluene solution. As for polymers comprised with donor and acceptor units, the absorption spectrum is characterized by two spectral features, a high-energy peak and a broad low-energy band.[41,51] The high-energy peak located at approximately 400 nm can be attributed to the π-π* transition in the polymeric backbone. The low-energy band with major absorption peak at 678 nm for C1 and 684 nm for C3, respectively, is ascribed to the charge-transfer (CT) transition between electron-donating ethylene units and the electron-deficient NDI units. In the solid state, the main absorption bands become broader, and the red shifts occur with maximum absorption peaks at 716 nm and 726 nm by 38 nm and 42 nm relative to that in solution, for C1 and C3 respectively. These large red shifts from solution to thin film are indicative of a planarization of conjugated backbone and strong interchain π-π stacking in the solid state. Notably, the absorption spectra of C3 film exhibits a sharp shoulder peak at 805 nm while that of C1 film doesn't, which may originate from more efficient stacking in polymer C3. The absorption edges (λ_{onset}) of the two polymer films are 890 nm for C1 and 895 nm for C3, from which the optical band gaps (E_g^{opt}) of polymers can be calculated according to $E_g^{opt} = 1240/\lambda_{onset}$. E_g^{opt} values of C1 and C3 are 1.40 and 1.38 eV, respectively.

Cyclic voltammetry measurement was carried out to evaluate the electrochemical properties and estimate the HOMO/LUMO energy levels of two polymers (Fig. S1). Our test results is similar to the data of previous work by Liu et al.[38] As we expected, the changes of alkyl-chain branching position have a negligible effect on polymer energy levels.[28-31,35] As listed in Table 1 and Fig. 2b, the HOMO/LUMO energy values of C1 and C3 are -5.61/-3.93 eV and -5.61/-3.94 eV. The energy levels of polymer are well matched with polymer PBDTTT-C-T[52] and the LUMO energy are significantly higher-lying than that of $PC_{70}BM$ (Fig. 2b); thus, a large V_{oc} could be expected to occur in their corresponding devices.

GIXD Characterization

To study the effect of alkyl-chain branching position of the polymers on the packing orientation and crystallinity of films, grazing incidence X-ray diffraction (GIXD) were performed. As seen in Fig. 3 and Fig. S3, an edge-on orientation was found for both thin films, with evident (100) diffraction peaks in the out-plane direction. The d_{100}-spacings corresponding to out-plane space distance between polymer backbones are 23.2 Å for C1 and 26.0 Å for C3, respectively. This kind of space related to the side chain length is much shorter than that of fully extended alkyl chains, indicating that side chains of polymer in adjacent layers were closely interdigitated in lamellar structures.[23,53] Noticeably, an obvious (200) diffractions at 6.80° and (001) diffraction halos of alkyl-chain[38] at 5.68° for polymer C3 demonstrate that polymer C3 possesses superior crystallinity ability compared with polymer C1. Therefore, moving the branching position away from the conjugated backbone may decline the steric effect of bulk octyldecyl chain and promote the ordering of lamellar structure of polymer.

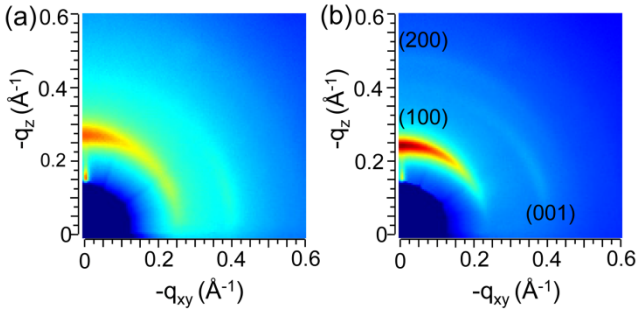

Fig. 3 2D GIXS patterns of C1 (a) and C3 (b) thin films.

Photovoltaic properties

All-polymer solar cells were fabricated by employing C1 or C3 as acceptor material and PBDTTT-C-T as donor material (Fig. 1), with a conventional device structure of ITO/PEDOT:PSS/PBDTTT-C-T:polymer/Ca/Al. The best weight ratio of PBDTTT-C-T:polymer was 1:1 (w/w). Fig. 4a displayed the current density-voltage (*J-V*) curves of the devices under illumination of AM 1.5 G simulated white light with anintensity of 100 mW cm^{-2}. The V_{oc}, short circuit current density (J_{sc}), fill factor (FF) and PCE of the devices are showed in Table 2 and Fig. 4. The other device data are summarized in the Supporting Information.

Devices fabricated from a blend of C1 with PBDTTT-C-T harvested a J_{sc} of 3.64 mA/cm^2, a V_{oc} of 0.81 V and a FF of 0.49, corresponding to a PCEs of 1.21%. When linear chain increased to three carbon atoms in C3, devices showed a little improvement on the photovoltaic performance up to a PCE of 1.27%, which indirectly demonstrated that molecular weight has little effect on photovoltaic performance. In order to further improve the PCE, DIO was used as a processing additive.[54-56] When 1% DIO was added, the photovoltaic performance based on C1 was further improved to 1.68%, with a J_{sc} of 3.64 mA/cm^2; the highest PCE of 1.92% was achieved by adding 3% DIO to PBDTTT-C-T/C3 devices, with a highest J_{sc} of 4.70 mA/cm^2. However, further increasing the ratio of DIO resulted in a gradual decrease in photovoltaic performance for both C1 and C3 (Table S1). Charge motilities of the optimal blend films based on polymer C1 and C3 were measured using the charge only SCLC method showed in Fig. S4. Hole and the electron

mobilities of PBDTTT-C-T:polymer BHJ devices were estimated to be 1.3×10^{-4} cm^2 V^{-1} s^{-1} and 6.6×10^{-5} cm^2 V^{-1} s^{-1} for C1, and 1.8×10^{-4} cm^2 V^{-1} s^{-1} and 1.0×10^{-4} cm^2 V^{-1} s^{-1} for C3, respectively. It is noteworthy that electron mobility in C3-based active layers is much higher than that based on C1, and equal to its hole mobility value. The balanced hole and electron motilities in the C3-based blend film can largely explain the high performance of the BHJ solar cells.[2] On account of the very close V_{oc} and FF, improvement of the efficiency is mainly from the enhanced J_{sc} and high electron mobility, which probably linked to the optimized morphology of the blend film (vide infra).

Moreover, improvement of the J_{sc} is supported by the external quantum efficiency (EQE) responses (Fig. 5b), in which the addition of DIO yields an increase of the EQE response. As for the PBDTTT-C-T/C1 device, 1% DIO additive greatly improved the maximum monochromic EQE from 13.4% to 18.0 % at 720 nm. After further manipulating the alkyl-chain branching position, the maximum value reached 19.6% at 640 nm under the optimal condition, consistent with the highest J_{sc}.

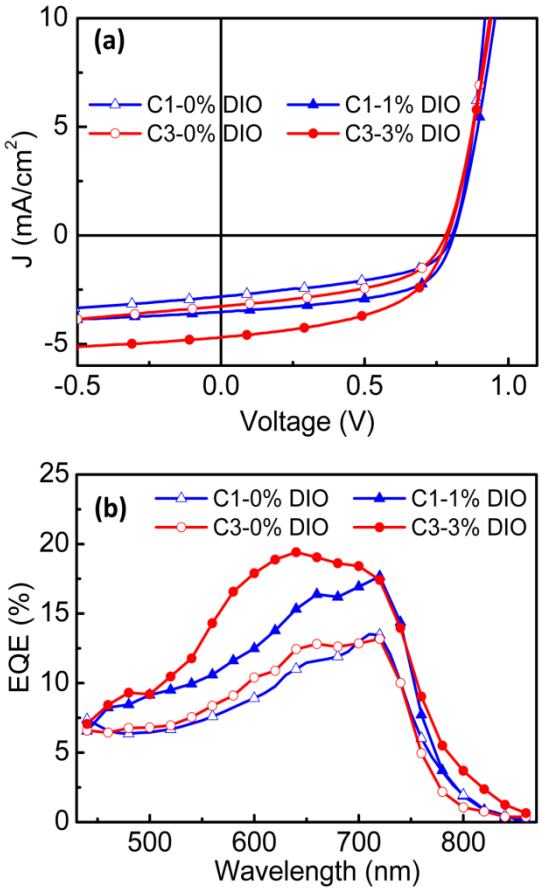

Fig. 4 The current density (*J*)–voltage (*V*) curves (a) and the typical EQE curves (b) of the devices under different conditions.

Morphology Characterization

The TEM and AFM was used to study the phase separation in blend films (processed with DCB or DCB:DIO solvent).The TEM images of the blend films are shown in Fig. 5, and the corresponding AFM images are provided in Fig. S3. In TEM image, the dark regions could be attributed to the acceptor (C1 or C3) domains, while the bright regions could be attributed to the donor (PBDTTT-C-T) domains (depicted in Fig. S4). When no DIO is added, blend films based on C1 and C3 show both dark aggregation domains and small phase separation, which indicates that the poor performances in polymers C1 and C3 are related to the non-optimized morphologies. The PBDTTT-C-T/C3 blend film exhibits more and bigger aggregation domains (ca. 15 nm size) than PBDTTT-C-T/C1 blend film. The aggregation domains may originate from its better crystallinity ability, while polymer PBDTTT-C-T is non-crystalline.[52,57] The small improvement of PCE for polymer C1 and C3 indicates that polymer crystallinity cannot be the sole factor influencing the performance of devices. Other factors, like the phase domain sizes and ordering of polymer aggregation in the BHJ blends, may also be important because the exciton separation and charge mobility should be efficient across the entire active layer. It is well proved that addition of small-molecule additives

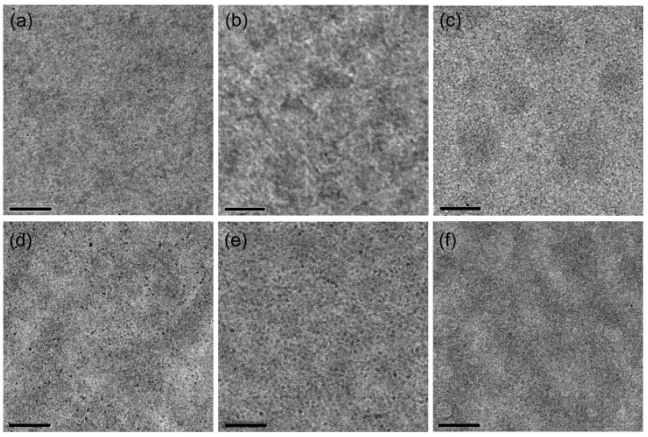

Fig. 5 TEM images of blend films: PBDTTT-C-T:C1 with (a) 0% DIO, (b) 1% DIO, (c) 2% DIO; PBDTTT-C-T:C3 with (d) 0 % DIO, (e) 3% DIO and (f) 4% DIO. The scale bar is 200 nm.

Table 2 Photovoltaic performances of all-PSCs devices based on the two polymers with DCB as solvent and DIO as processing additive

Cn[a]	Solvent(DCB:DIO)[b]	J_{sc}[c] (mA/cm^2)c	V_{oc}[c] (V)	FF[c] (%)	PCE[c] (%) (best[d])
C1	100:0	2.88±0.13	0.81±0.01	47.63±1.65	1.11±0.08 (1.21)
	99:1	3.56±0.04	0.81±0.00	55.04±1.91	1.59±0.06 (1.68)
C3	100:0	3.17±0.09	0.78±0.01	50.65±0.60	1.24±0.03 (1.27)
	97:3	4.75±0.11	0.79±0.01	49.29±1.33	1.85±0.05 (1.92)

[a]Cn:donor= 1:1 (w/w); [b]DCB:DIO (v/v); [c]Only the optimized recipes were considered for the estimation of the average PCE; data have been averaged on different devices (see supporting information). [d]The performance of the best device is given in parentheses. The active area of the device was 0.06 cm^2.

DIO into the solvent would optimize the blend morphology in BHJ polymer solar cells.[56,58-60] After 1% DIO is added, PBDTTT/C1 blend film exhibits a continuous interpenetrating network with nanoscale phase segregation. Simultaneously, PBDTTT-C-T/C3 blend film exhibits clear nonascale phase separation and lots of dark spots (ca. 20 nm size), which relates to the solubility and crystallization of polymer C3. In all-polymer system, the polymer crystallinity would be an important driving force to form the acceptor domains in this work. With the slow evaporation speed of DIO, it provides sufficient time for polymer C3 to aggregate gradually and form the nanoscale phase separation.[56,61] The nanoscale phase separation provides large D/A interfaces and efficient channels for charge transport, thus leading to high J_{sc} and charge mobility, especially the electron mobility. Moreover, the observation in TEM images can also be confirmed by AFM measurements (see Fig. S3). These results demonstrate that the alkyl-chain branching position significantly influences the nanoscale morphology of blend films by improving polymer crystallinity. Polymer with superior crystallinity could be easy to aggregate in blends, thus forming the nanoscale morphology.

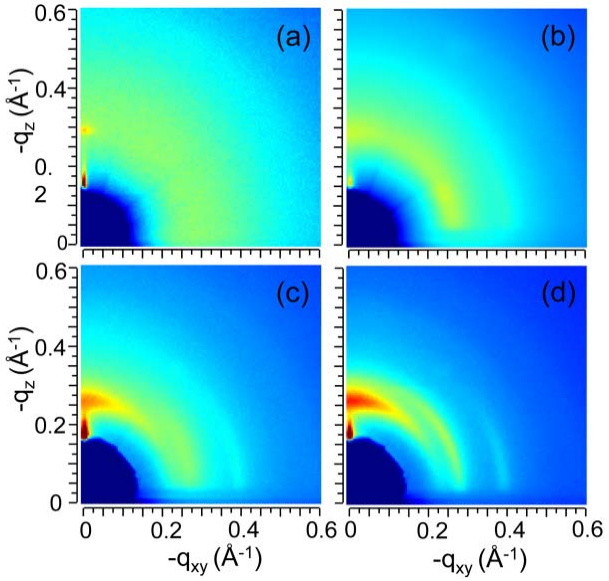

Fig. 6 2D GIXS patterns of blend films: donor:C1 with 0% DIO (a) and 1% DIO (b); donor:C3 with 0% DIO (c) and 3% DIO (d).

GIXS was used to provide the structural ordering of two polymers in blend films (processed with DCB or DCB:DIO mixture solvent) in Fig. 6. The PBDTTT-C-T:C1 blend film shows ambiguous diffraction arcs; however, the PBDTTT-C-T:C3 blend film shows much clear diffraction arcs. This indicates that polymer C3 in the BHJ blend is higher ordered than that of polymer C1, which well matches with the crystallinity of two polymers. The thin films processed from DCB and DCB:DIO mixture solvent yield the similar results, which suggested DIO is benifical to the aggregation of two polymers. When the film are casted from DCB:DIO (97:3,v/v), several arcs appeared in Fig. 6d demonstrate that polymer C3 distributes with highly ordered structure in the BHJ blend film, which enhances the electron transport ability. The clear diffraction arcs in Fig. 6d also provides an additional evidence for the clear nanoscale phase separation and aggregation of acceptor C3. Consequently, moving the branching position further from the main chain could promote the performance of devices by realizing the nanoscale morphology and high ordering structure of polymer.

Conclusions

In conclusion, two polymers based on NDI with different alkyl-chain branching position, C1 and C3, were synthesized and characterized. It was proved out that the location of the branching point had significant effect on their optical absorption, conjugated backbone orientation, crystallinity, device morphology and charge mobility. Moving the branching position away from the backbone resulted in superior crystallinity of C3. From C1 to C3, the morphology in optimal device showed improved nanoscale morphology and high ordering structure of polymer. Hence, all-PSCs based on C3 showed a higher PCE of 1.92%, while 1.68% for C1. Therefore, manipulation of alkyl-chain branching position provides new insights into the design of optimum polymers as acceptor for high performance in all-PSCs.

Acknowledgements

The GIXD data were obtained at 1W1A, Beijing Synchrotron Radiation Facility. The authors gratefully acknowledge the assistance of scientists of Diffuse X-ray Scattering Station during the experiments. This work was supported by the National Natural Science Foundation of China (No. 20925309, 21190034, 21221002, 21203212) and the National Research Fund for Fundamental Key Project 973 (2011CB808402, 2013CB933500).

Notes and references

[a] Beijing National Laboratory for Molecular Sciences (BNLMS), Institute of Chemistry, Chinese Academy of Sciences, Beijing, 100190, P. R. China. E-mail: hongbing.fu@iccas.ac.cn.;chunlgu@iccas.ac.cn.
[b] University Chinese Academy of Sciences, Beijing 100049, P. R. China.

Electronic Supplementary Information (ESI) available: [details of for the measurement of cyclic voltammogram and charge mobilities, TGA images and AFM images]. See DOI: 10.1039/b000000x/

1 Y. Zhou, T. Kurosawa, W. Ma, Y. Guo, L. Fang, K. Vandewal, Y. Diao, C. Wang, Q. Yan, J. Reinspach, J. Mei, A. L. Appleton, G. I. Koleilat, Y. Gao, S. C. B. Mannsfeld, A. Salleo, H. Ade, D. Zhao and Z. Bao, *Adv. Mater.*, 2014, **26**, 3767.
2 T. Earmme, Y.-J. Hwang, N. M. Murari, S. Subramaniyan and S. A. Jenekhe, *J. Am. Chem. Soc.*, 2013, **135**, 14960.
3 G. Dennler, M. C. Scharber and C. J. Brabec, *Adv. Mater.*, 2009, **21**, 1323.
4 M. Schubert, D. Dolfen, J. Frisch, S. Roland, R. Steyrleuthner, B. Stiller, Z. Chen, U. Scherf, N. Koch, A. Facchetti and D. Neher, *Adv. Energy Mater.*, 2012, **2**, 369.

5 B. C. Thompson and J. M. J. Fréchet, *Angew. Chem. Int. Ed.*, 2008, **47**, 58.
6 E. Zhou, J. Cong, Q. Wei, K. Tajima, C. Yang and K. Hashimoto, *Angew. Chem. Int. Ed.*, 2011, **50**, 2799.
7 W. Yu, D. Yang, X. Zhu, X. Wang, G. Tu, D. Fan, J. Zhang and C. Li, *ACS Appl. Mater. Interfaces*, 2014, **6**, 2350.
8 D. Mori, H. Benten, I. Okada, H. Ohkita and S. Ito, *Energy Environ. Sci.*, 2014, **7**, 2939.
9 Y. Zhou, T. Kurosawa, W. Ma, Y. Guo, L. Fang, K. Vandewal, Y. Diao, C. Wang, Q. Yan, J. Reinspach, J. Mei, A. L. Appleton, G. I. Koleilat, Y. Gao, S. C. B. Mannsfeld, A. Salleo, H. Ade, D. Zhao and Z. Bao, *Adv. Mater.*, 2014, **26**, 3767.
10 D. Mori, H. Benten, J. Kosaka, H. Ohkita, S. Ito and K. Miyake, *ACS Appl. Mater. Interfaces*, 2011, **3**, 2924.
11 E. Zhou, J. Cong, K. Hashimoto and K. Tajima, *Adv. Mater.*, 2013, **25**, 6991.
12 A. C. Arias, J. D. MacKenzie, R. Stevenson, J. J. M. Halls, M. Inbasekaran, E. P. Woo, D. Richards and R. H. Friend, *Macromolecules*, 2001, **34**, 6005.
13 C. R. McNeill, A. Abrusci, I. Hwang, M. A. Ruderer, P. Müller-Buschbaum and N. C. Greenham, *Adv. Funct. Mater.*, 2009, **19**, 3103.
14 C. R. McNeill and N. C. Greenham, *Adv. Mater.*, 2009, **21**, 3840.
15 M. M. Wienk, J. M. Kroon, W. J. H. Verhees, J. Knol, J. C. Hummelen, P. A. van Hal and R. A. J. Janssen, *Angew. Chem. Int. Ed.*, 2003, **42**, 3371.
16 A. C. Arias, N. Corcoran, M. Banach, R. H. Friend, J. D. MacKenzie and W. T. S. Huck, *Appl. Phys. Lett.*, 2002, **80**, 1695.
17 H. N. Tsao, D. M. Cho, I. Park, M. R. Hansen, A. Mavrinskiy, D. Y. Yoon, R. Graf, W. Pisula, H. W. Spiess and K. Müllen, *J. Am. Chem. Soc.*, 2011, **133**, 2605.
18 J. Mei and Z. Bao, *Chem. Mater.*, 2013, **26**, 604.
19 P. M. Beaujuge and J. M. J. Fréchet, *J. Am. Chem. Soc.*, 2011, **133**, 20009.
20 J. Mei, D. H. Kim, A. L. Ayzner, M. F. Toney and Z. Bao, *J. Am. Chem. Soc.*, 2011, **133**, 20130.
21 H. Sirringhaus, P. J. Brown, R. H. Friend, M. M. Nielsen, K. Bechgaard, B. M. W. Langeveld-Voss, A. J. H. Spiering, R. A. J. Janssen, E. W. Meijer, P. Herwig and D. M. de Leeuw, *Nature*, 1999, **401**, 685.
22 I. McCulloch, M. Heeney, C. Bailey, K. Genevicius, I. MacDonald, M. Shkunov, D. Sparrowe, S. Tierney, R. Wagner, W. Zhang, M. L. Chabinyc, R. J. Kline, M. D. McGehee and M. F. Toney, *Nat. Mater.*, 2006, **5**, 328.
23 B. S. Ong, Y. Wu, P. Liu and S. Gardner, *J. Am. Chem. Soc.*, 2004, **126**, 3378.
24 F. Zhang, Y. Hu, T. Schuettfort, C. Di, X. Gao, C. R. McNeill, L. Thomsen, S. C. B. Mannsfeld, W. Yuan, H. Sirringhaus and D. Zhu, *J. Am. Chem. Soc.*, 2013, **135**, 2338.
25 M. S. Chen, J. R. Niskala, D. A. Unruh, C. K. Chu, O. P. Lee and J. M. J. Fréchet, *Chem. Mater.*, 2013, **25**, 4088.
26 A. C. Mayer, M. F. Toney, S. R. Scully, J. Rivnay, C. J. Brabec, M. Scharber, M. Koppe, M. Heeney, I. McCulloch and M. D. McGehee, *Adv. Funct. Mater.*, 2009, **19**, 1173.
27 N. Wang, Z. Chen, W. Wei and Z. Jiang, *J. Am. Chem. Soc.*, 2013, **135**, 17060.
28 I. Osaka, M. Saito, T. Koganezawa and K. Takimiya, *Adv. Mater.*, 2014, **26**, 331.
29 I. Meager, R. S. Ashraf, S. Mollinger, B. C. Schroeder, H. Bronstein, D. Beatrup, M. S. Vezie, T. Kirchartz, A. Salleo, J. Nelson and I. McCulloch, *J. Am. Chem. Soc.*, 2013, **135**, 11537.
30 C. Piliego, T. W. Holcombe, J. D. Douglas, C. H. Woo, P. M. Beaujuge and J. M. J. Fréchet, *J. Am. Chem. Soc.*, 2010, **132**, 7595.
31 Y. Liang and L. Yu, *Acc. Chem. Res.*, 2010, **43**, 1227.
32 J. Warnan, C. Cabanetos, R. Bude, A. El Labban, L. Li and P. M. Beaujuge, *Chem. Mater.*, 2014, **26**, 2829.
33 C. Cabanetos, A. El Labban, J. A. Bartelt, J. D. Douglas, W. R. Mateker, J. M. J. Fréchet, M. D. McGehee and P. M. Beaujuge, *J. Am. Chem. Soc.*, 2013, **135**, 4656.
34 S. Subramaniyan, H. Xin, F. S. Kim, S. Shoaee, J. R. Durrant and S. A. Jenekhe, *Adv. Energy Mater.*, 2011, **1**, 854.
35 T. W. H. Claudia Piliego, Jessica D. Douglas, Claire H. Woo, Pierre M. Beaujuge, and Jean M. J. Fréchet, *J. Am. Chem. Soc.*, 2010, **132**, 3.
36 X. Guo and M. D. Watson, *Org. Lett.*, 2008, **10**, 5333.
37 C. Gu, W. Hu, J. Yao and H. Fu, *Chem. Mater.*, 2013, **25**, 2178.
38 H. Chen, Y. Guo, Z. Mao, G. Yu, J. Huang, Y. Zhao and Y. Liu, *Chem. Mater.*, 2013, **25**, 3589.
39 K. Tremel, F. S. U. Fischer, N. Kayunkid, R. D. Pietro, R. Tkachov, A. Kiriy, D. Neher, S. Ludwigs and M. Brinkmann, *Adv. Energy Mater.*, 2014, **4**, 1301659.
40 Y. Kim, J. Hong, J. H. Oh and C. Yang, *Chem. Mater.*, 2013, **25**, 3251.
41 R. Steyrleuthner, R. Di Pietro, B. A. Collins, F. Polzer, S. Himmelberger, M. Schubert, Z. Chen, S. Zhang, A. Salleo, H. Ade, A. Facchetti and D. Neher, *J. Am. Chem. Soc.*, 2014, **136**, 4245.
42 A. Luzio, D. Fazzi, D. Natali, E. Giussani, K.-J. Baeg, Z. Chen, Y.-Y. Noh, A. Facchetti and M. Caironi, *Adv. Funct. Mater.*, 2014, **24**, 1151.
43 S. Fabiano, Z. Chen, S. Vahedi, A. Facchetti, B. Pignataro and M. A. Loi, *J. Mater. Chem.*, 2011, **21**, 5891.
44 Y.-J. Hwang, G. Ren, N. M. Murari and S. A. Jenekhe, *Macromolecules*, 2012, **45**, 9056.
45 Z.-K. Tan, K. Johnson, Y. Vaynzof, A. A. Bakulin, L.-L. Chua, P. K. H. Ho and R. H. Friend, *Adv. Mater.*, 2013, **25**, 4131.
46 T. W. Holcombe, J. E. Norton, J. Rivnay, C. H. Woo, L. Goris, C. Piliego, G. Griffini, A. Sellinger, J.-L. Brédas, A. Salleo and J. M. J. Fréchet, *J. Am. Chem. Soc.*, 2011, **133**, 12106.
47 J. R. Moore, S. Albert-Seifried, A. Rao, S. Massip, B. Watts, D. J. Morgan, R. H. Friend, C. R. McNeill and H. Sirringhaus, *Adv. Energy Mater.*, 2011, **1**, 230.
48 P. Liu, K. Zhang, F. Liu, Y. Jin, S. Liu, T. P. Russell, H.-L. Yip, F. Huang and Y. Cao, *Chem. Mater.*, 2014, **26**, 3009.
49 W. Li, L. Yang, J. R. Tumbleston, L. Yan, H. Ade and W. You, *Adv. Mater.*, 2014, **26**, 4456.
50 X. Xu, Y. Wu, J. Fang, Z. Li, Z. Wang, Y. Li and Q. Peng, *Chem. Eur. J.*, 2014, 1.
51 K. G. Jespersen, W. J. D. Beenken, Y. Zaushitsyn, A. Yartsev, M. Andersson, T. Pullerits and V. Sundström, *J. Chem. Phys.*, 2004, **121**, 12613.
52 L. Huo, S. Zhang, X. Guo, F. Xu, Y. Li and J. Hou, *Angew. Chem.*, 2011, **123**, 9871.
53 Y. Li, S. P. Singh and P. Sonar, *Adv. Mater.*, 2010, **22**, 4862.
54 J. Peet, J. Y. Kim, N. E. Coates, W. L. Ma, D. Moses, A. J. Heeger and G. C. Bazan, *Nat. Mater.*, 2007, **6**, 497.

55 M. Han, H. Kim, H. Seo, B. Ma and J.-W. Park, *Adv. Mater.*, 2012, **24**, 6311.
56 J. K. Lee, W. L. Ma, C. J. Brabec, J. Yuen, J. S. Moon, J. Y. Kim, K. Lee, G. C. Bazan and A. J. Heeger, *J. Am. Chem. Soc.*, 2008, **130**, 3619.
57 L. Huo, L. Ye, Y. Wu, Z. Li, X. Guo, M. Zhang, S. Zhang and J. Hou, *Macromolecules*, 2012, **45**, 6923.
58 J. J. Jasieniak, B. B. Y. Hsu, C. J. Takacs, G. C. Welch, G. C. Bazan, D. Moses and A. J. Heeger, *Acs Nano*, 2012, **6**, 8735.
59 L. Gang, Z. Rui and Y. Yang, *Nat. Photonics*, 2012, **6**, 153.
60 J. Peet, M. L. Senatore, A. J. Heeger and G. C. Bazan, *Adv. Mater.*, 2009, **21**, 1521.
61 J. Huang, C. Zhan, X. Zhang, Y. Zhao, Z. Lu, H. Jia, B. Jiang, J. Ye, S. Zhang, A. Tang, Y. Liu, Q. Pei and J. Yao, *ACS Appl. Mater. Interfaces*, 2013, **5**, 2033.